Further Investigation into Geometric Accuracy of DMC

International Calibration and Orientation Workshop

January 30th – February 1st, 2008, Castelldefels, Spain

Mostafa Madani, Ilya Shkolnikov

Intergraph Corporation, Alabama, USA

E-mail: mostafa.madani@intergraph.com, ilya.shkolnikov@intergraph.com

Keywords: Digital aerial cameras, Camera Calibration, Self-calibration, Geometric Correction

ABSTRACT

Digital Mapping Camera (DMC) has been introduced into the market in early 2003. Since then, multiple projects have been successfully flown by different customers all over the world. All these DMC projects achieved the required accuracy standards for different photogrammetric applications established by several organizations such as ASPRS, NMAS, etc. However, some DMC users and research institutions have indicated that there is still a small systematic error left in the DMC virtual images that can be modelled by "special additional parameters" in a self-calibration bundle adjustment. Results of the self-calibration bundle adjustments and their distortion models cannot easily be used or implemented directly into the real-time mathematical models of almost any softcopy system. In addition, not all photogrammetric organizations have appropriate bundle adjustment programs and technical staffs to perform such aerial triangulations. Furthermore, some DMC users only deliver virtual images to their customers, and they do not process or get into any photogrammetric applications. Therefore, a better and simpler procedure is needed to allow DMC owners to produce "distortion free" virtual images.

In this paper, two methods to model the "remaining" systematic errors of DMC VIR imagery are explained. Correction grids for virtual images of test blocks are generated either by collocation adjustment or self-calibration bundle adjustment. The existing DMC users optionally can generate "distortion" free virtual imagery by applying these correction grids during the post-processing step. The correction grids will also be used to refine the calibration certificate of new DMCs. Furthermore, correction grids can also be used in the real-time math model of the ImageStation products. Three DMC test blocks are used for this investigation. Correction grids generated by collocation and self-calibration are used and new virtual images are generated. The new VIR imagery does not show any significant distortion in imagery or any DTM bending.

1. INTRODUCTION

Aerial cameras have been successfully used around the world for many decades. During the past two decades, the mapping sciences have progressively moved toward digital mapping, making use of multidisciplinary developments in the field of geomatics. Digital Mapping Camera (DMC), manufactured by Intergraph Corporation, represents one of the latest developmental steps in this long history (Dörstel 2003).

The DMC is based on Charge Coupled Device (CCD) frame (matrix) sensor technology, which provides a very high interior geometric stability. The camera is designed to perform under various light conditions within a wide range of exposure times. Features such as electronic Forward Motion Compensation (FMC) and 12-bit-per-pixel radiometric resolution for each of the panchromatic and color channel camera sensors provide the capabilities for operating even under

less than favourable flight conditions. The DMC can produce small-scale or large-scale images with ground resolutions of fewer than five centimeters.

The DMC consists of eight sensors: four panchromatic sensors and four multispectral sensors. The multispectral sensors are 3k x 2k in size, with one sensor capturing red data, one capturing blue data, one capturing green data, and one capturing near-infrared data. The four panchromatic sensors (Figure 1) each capture one image of a particular area (7k x 4k), which partly overlap one another.

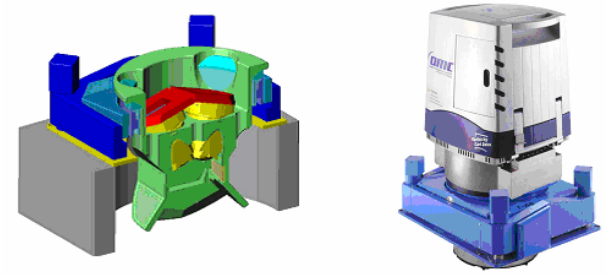

Figure 1. Lens cone with panchromatic camera head and DMC with gyro stabilized mount

The four images are captured from slightly different positions and synchronous in time to about 0.01 msec. They are subsequently used to produce one large image composite, 7680 x 13824 in size as shown in Figure 2.

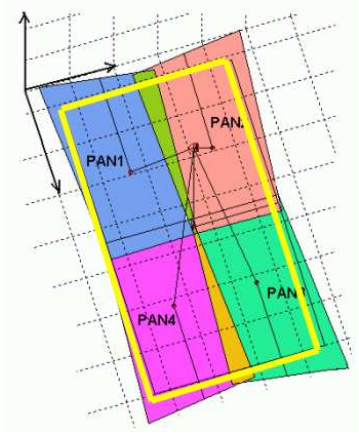

Figure 2. Footprint of 4 pan images projected into the virtual image (yellow area)

The image data that the camera captures is stored on a solid-state device (SSD) which is attached to the camera system. This storage unit can easily be detached from the DMC and replaced by an empty one during the photo flight.

The DMC Post-Processing Software (PPS) is used for producing virtual images from the raw image data. PPS is completed in two steps: radiometric processing and then geometric processing. Radiometric post-processing compensates for the effects of defect pixels, the individual sensitivity of each single CCD pixel, vignetting, the influence of aperture, and the filter influence (for correction on multi-spectral images). The intermediate images, generated from radiometric processing, are written to the intermediate RAID storage on the post-processing server. The intermediate images are then geometrically corrected for lens distortion based on a calibration of the individual camera heads and are subsequently combined to form the image

composite (Madani, al. 2004). The final output images are written to the output RAID storage designated for the final images on the post-processing server.
The PPS can produce several different types of output files. Full-resolution panchromatic image files are produced from images taken by the camera's four panchromatic sensors. Also, color and color-infrared output images can be produced using the full-resolution panchromatic imagery combined with the data from the multispectral sensors. This allows the possibility of producing four types of full resolution images (7680 x 13824): panchromatic, color, near-infrared, and 4-band.

2. DMC ERROR BUDGET

Lens-Chip distortion of each PAN camera contains about 93% unstable “linear” (magnification, shift) part and about 7% relatively stable “nonlinear” part. Magnification (focal length change) and shift (principle point change) of each PAN camera must be fully compensated (directly or indirectly) in the platform orientation of 4 PAN cameras. The uncompensated “nonlinear” part is the primary source of the systematic error, which directly propagates into virtual image rectification (VIR) camera space and affects platform orientation. The upper limit for the uncompensated distortion is about 2[um] which corresponds to about 8% of the total nonlinear distortion (24[um]). The estimated variation of the uncompensated nonlinear part with temperature is only 0.25[um]. So, the primary error source is a very stable constant term (Dörstel 2007).

Platform orientation, which is responsible for refinement to the relative orientation of 4 PAN cameras and compensation for “linear” part of the lens-chip distortion, is sensitive to uncompensated nonlinear error. However, a constant systematic effect from the primary error source on platform orientation produces a constant systematic response. Error in platform orientation that propagates to VIR image space as 4-quadrant perspective distortion is the secondary error source. In total, about 35% of the systematic error in VIR space is due to primary error source and 65% is due to secondary error source.

The minimal reliable estimate of the systematic distortion present in the DMC virtual panchromatic imagery by averaging all image residuals from block adjustment within a cell-grid placed on camera frame is about 0.5[um].The maximal observed distortion estimate is about 3-5[um] while random image feature measurement error due to radiometric noise is 2[um].

The unknown portion of the total systematic error in image space propagates into object space, causing block shape deformation (bending, twisting, wobbling, or similar). It is contributing to an increase in discrepancy on the vertical component of the check points by 3-4 times over the undistorted values achieved by the properly calibrated cameras or bundle block adjustment of DMC photos with 4-quadrant-based self-calibration. For example, for project “Rubi” (Alamus, 2006) with GSD of 10[cm], the Z residual is about 20[cm] versus 5[cm] when the cumulative image distortion is removed. For the reference, direct effect of 3[um] in image space contributes to only 0.6[cm] in object space for a single photo of this project scale; therefore, the rest of Z-distortion comes from the accumulated error causing block deformation. This deformation is visible as “banana curve” in Z-residuals of GPS observations along a strip with the relaxed statistical weights.

3. TECHNIQUES OF SYSTEMATIC ERROR COMPENSATION

Traditionally, cameras are calibrated in laboratories and satisfactory results for their component values are obtained. The main advantage of this method is the ease and convenience in testing camera components or properties of a particular material in the laboratory environment. Depending upon the degree of sophistication, calibration methods are commonly carried out in different ways (Madani, 1985):

- Pre-calibration (Laboratory)
- On-the-job (Test Field) calibration (camera intrinsic model)
- Self-calibration (Orthogonal polynomial model)
- A posteriori interpolation treatment of image residuals (Correction grid by Collocation)

3.1 Pre-calibration Method

As its name suggests, pre-calibration is completely separated from actual object photography. Calibration is usually carried out either by using laboratory equipment such as goniometers and collimator banks or by using special test areas of various ranges in sophistication. The mathematical model used in this method is normally based on the central projection equations, which are extended for interior orientation parameters and for radial and decentring lens distortion.

3.2 On-The-Job Calibration Method

On-The-Job (or, as it is sometimes called, Test Field) calibration is generally in closer conformance to operational circumstances than the laboratory calibration techniques. This approach requires an array of signalized and highly accurate control points, providing sufficient depth of field and high level of observational redundancy.

3.3 Self-Calibration Method

Unaccounted systematic errors may be expressed as the functional extension of the Collinearity equations (self-calibration). This approach differs significantly from the previous ones because it does not require object space control as such for calibration, except for the actual object point evaluation. Different mathematical models (physical, geometrical, or combinations of both) are used for expressing the unaccounted systematic errors.

Although simultaneous self-calibration is recognized as the most efficient technique for compensation of systematic errors, there are certain problems which still have to be solved. Some of these problems are:

- Treatment of APs as block or photo invariants or combinations of both
- Operational problems; that is, the total strategy of assessing blunders, errors in control points, and systematic errors
- The determinability checking of APs; that is, excluding indeterminable APs from the system.
- Significance testing of APs.

Each one of the above issues requires careful evaluation and proper use of the APs. The successful solution of the normal equations of the self-calibrating bundle adjustment is governed by the extent of correlation between the unknown parameters (AP coefficients, exterior orientation (EO) parameters, and object coordinates). If any two parameters, for instance, are highly correlated, both tend to perform the same function. In such a case, one or the other can be suppressed without losing much information. Therefore, it is very important to study the correlation structure of unknown parameters and to check the determinability of APs.

Common practice shows that for large-scale and precise engineering blocks, self-calibration bundle adjustment is required. Self-calibration APs compensate for the remaining distortion in both object space and image space of a single camera. DMC has 4 physical PAN sensors; therefore, only a 4-quadrant self-calibration of VIR imagery may become truly effective (Kruck, 2006, Riesinger, 2006, Honkavaara, 2006, Jacobsen, 2007). However, the only purpose of such self-calibration is to “unbend” the block during triangulation. For the sake of better accuracy in object space, self-calibration may significantly over-compensate the actual distortion in image space at the frame edges. Also, it is very dependent on given object space distortions. Therefore, under no circumstances such correction function should be used in post-orientation math or applied directly to VIR production. A reason for such overcompensation is that the polynomial

model has been derived to effectively compensate systematic distortions in areas concentrated around so-called Von Gruber centers of 5x5 or similar arrangement in camera frame format.

3.4 Correction Grid by Collocation Fit to Residual Trend

This method does not belong to the camera calibration methods mentioned above. In this method, some a posteriori interpolation treatment is performed on the image residuals of a bundle block adjustment. Calculated mean image residuals then serve as correction values at the interpolation points of the grid. The correction grid is able to remove the systematic errors in the image plane that could not be computed or modelled by APs in a self-calibration bundle adjustment. This correction grid application works the same way as "Reseau" to refine image coordinates for the local systematic errors by bi-linear interpolation.

4. FLIGHT SPECIFICATIONS FOR CORRECTION GRID CALIBRATION

In order to create a reliable correction grid array, a highly accurate ABGPS aerial photography of about 200 to 400 images having 60-80% forward overlap and 80% side overlap, with ground sample distance (GSD) of 5-10, 10-20, 20-40[cm], and with a reasonable number of well-distributed ground control points is required. In this case, 3 correction grids can be computed for these three different GSDs. Then VIR images of other blocks having GSDs within this range will be corrected by interpolation of these 3 grids. In case just one flight has been planned, it is recommended to use 10[cm] GSD to make a single correction grid to be used for other image scales. The procedure to create the correction grid is as follows:

a) Perform bundle block adjustment on a block of virtual images (tight GPS/control constraints and loose image constraints).
b) Compute mean image residuals per square cell (about 256x256 pixels). Each image cell should have at least 40 points in order to have a reliable correction grid.
c) Compute some sort of smoothing of the trend surface by either low-pass Gaussian kernel or least square surface splines.
d) Refine image coordinates with this "Correction Grid" using bi-linear interpolation.
e) Repeat steps (a-d) 3 to 4 times until maximum residual trend increment per cell drops to lower than 0.5[um].
f) Use the correction grids in the DMC PPS to generate "distortion free" virtual images.

Alternatively, correction grids can be generated from self-calibration bundle adjustments. Exported correction grids should cover the entire virtual image format. Otherwise, image coordinates outside the correction grid must be extrapolated, which will give wrong results. These correction grids can be imported in the DMC PPS for refining virtual images.

A number of DMC blocks with different configurations are used for this study. General specifications of these blocks are given in Table 1.

Table 1. Project Specifications

DMC ID (Project Name)	**DMC 50**	**DMC 48**	**DMC 27**
Flying Height [m]	1000	800	750
GSD [cm]	10	8	7.5
% Forward Overlap	80	80	60
% Side Overlap	80	80	80
Number of Strips/Cross Strips	10 / 10	13 / 2	27 / 2
Number of Images	379	376	1105
Number of Control Points	8	21	39
Number of Check Points	6	20	14
Control Std Devs (X, Y, Z) [cm]	3, 3, 4	2, 2, 2	3, 3, 3
GPS Std Devs (X, Y, Z) [cm]	3, 3, 4	3, 3, 3	5, 5, 5

5. NUMERICAL RESULTS

5.1 DMC 50 Calibration and Testing

ImageStation Automatic Triangulation is used to generate tie/pass points (Madani, 2001). This block is then adjusted by using GPS with block shift correction (no IMU is used) and 10 microns for standard deviation of image points. The general adjustment statistics are given in Table 2, and distributions of control/check points and adjusted object points are given in Figure 3 and Figure 4.
.

Table 2. DMC50 general adjustment statistics

Sigma =2.9[um], RMS x=2.7, RMS y = 2.6[um]	X[m]	Y[m]	Z[m]
RMS of 8 Control Points	0.017	0.029	0.019
RMS of 6 Check Points	0.020	0.032	0.047
MAX of 8 Control Points	0.035	0.043	0.030
MAX of 6 Check Points	0.036	0.049	0.067
RMS GPS	0.007	0.009	0.019
GPS Block Shift	-0.028	-0.033	0.218

Distributions of control/check points and adjusted object points are given in Figure 3 and Figure 4.

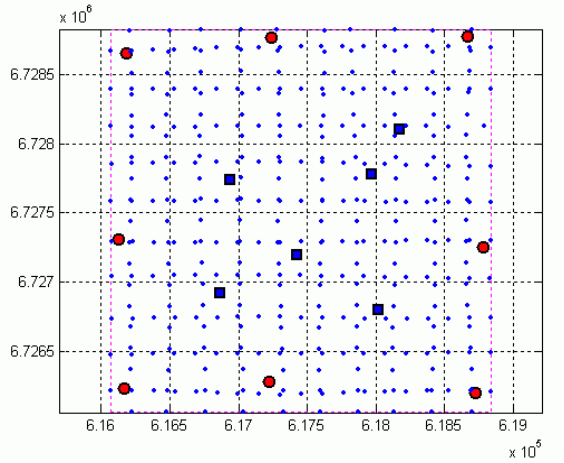

Figure 3. Distribution of control “red circles”, check “blue squares”, and photo centers “red circles”

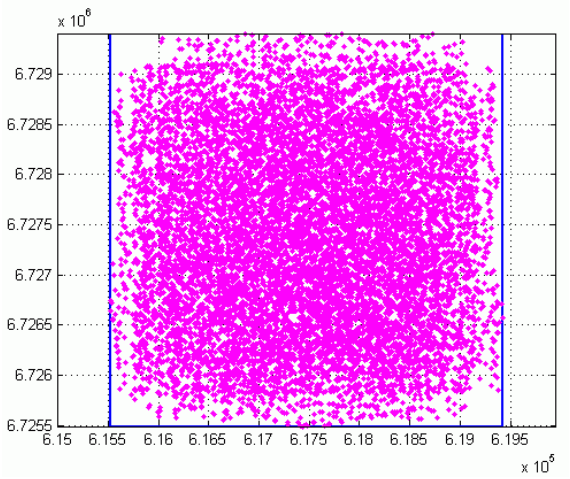

Figure 4. Distribution of adjusted object points

This block is considered a reference block, which gives the best estimate of the terrain (true DTM shape). Tight GPS constraints and loose image constraints squeeze all existing geometric discrepancy into image residuals where collocation fit must capture its average-per-block systematic trend. The resulting distortion-free block will not be any more accurate in Z component than this reference block.

5.1.1 Correction Grid generation

For reliable estimation of the residual trend surface that is almost free from influence of clusters of small outliers, the recommended density of image residuals per 256x256-pixel cell should be

between 20 to 40 points. A histogram of image points per cell and spatial distribution of cumulative redundancy number per cell (which serves as weight factor in collocation fit) are given in Figure 5.

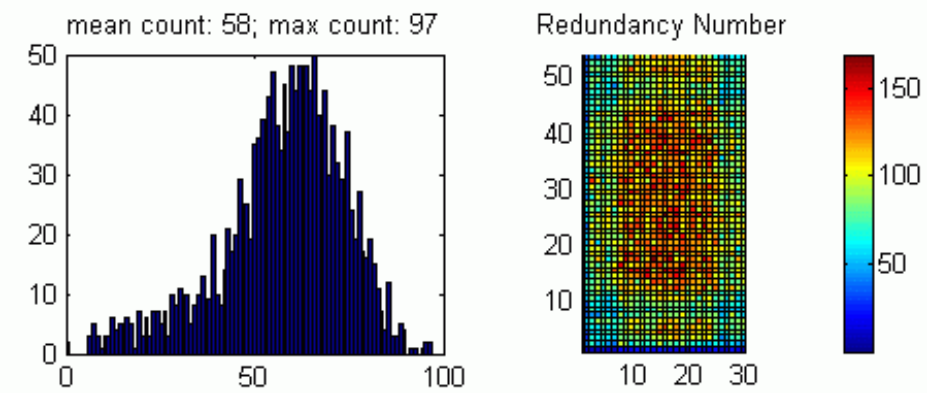

Figure 5. Histogram of image points and cumulative redundancy number distribution per cell

The collocation fit has converged to a trend surface after 4 iterations performed with the previously adjusted reference block. The estimated systematic distortion and the remaining residual trend are given in Figure 6.

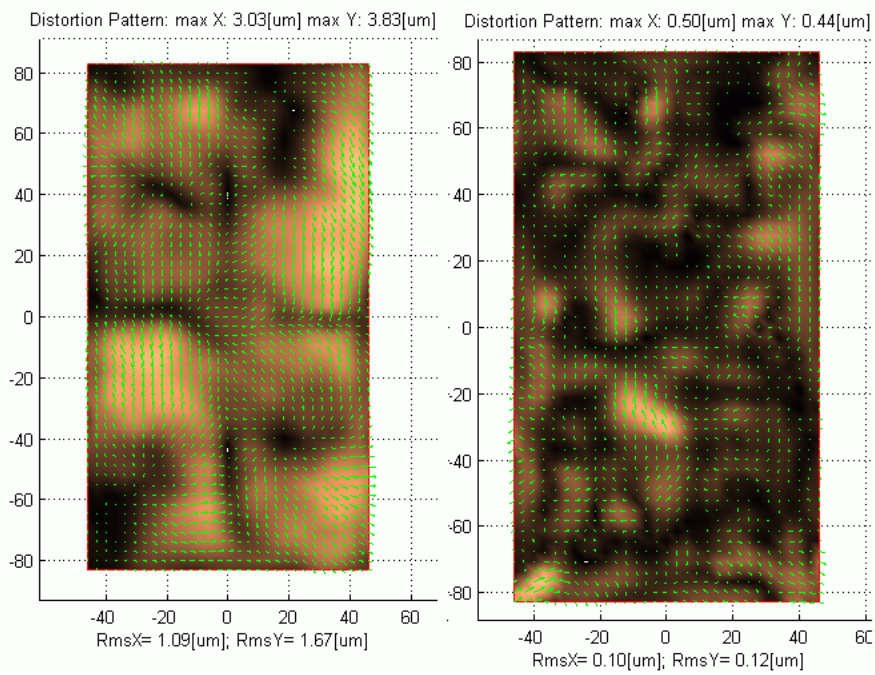

Figure 6. DMC 50 VIR correction grid and the remaining distortion trend

As one can observe, the maximal estimated distortion per component (x or y) is 3.83[micron] or 0.32[pixel]. The result of the bundle adjustment of this calibration block using refined image coordinates and with standard deviation of 2 microns is given in Table 3. RMS Z values have virtually not changed after collocation fit, which is usually the case since the collocation trend simply subtracted the systematic part leaving random error virtually in the same least-squares state.

5.1.2 Post-Correction Analysis of a Test Block

The main goal of the DMC VIR correction grid is to reduce DTM block bending in Z. Generally, it cannot improve much RMS of the check points in a block with dominant local deformations. Therefore, the only reliable estimate of the improvement in DTM shape achieved after grid correction is to monitor a mean trend difference between some reference DTM shape and the test block shape, before and after correction. This particular block constitutes a situation when one cannot trust very sparse check point statistics and must rely on the mean trend estimate.

Table 3. DMC50 calibration block adjustment statistics

Sigma=2.5[um],RMS x = 2.4, RMS y = 2.2[um]	X[m]	Y[m]	Z[m]
RMS of 8 control points	0.017	0.027	0.021
RMS of 6 check points	0.018	0.029	0.036
MAX of 8 control points	0.032	0.042	0.037
MAX of 6 check points	0.026	0.048	0.052
RMS GPS	0.033	0.040	0.025
GPS Block Shift	-0.029	-0.032	0.219

In lieu of a separate test block, a sub-block of the DMC50 project with 4 strips, 38 images, and 60% / 30% overlaps is selected. Automatic aerial triangulation is run on this selected sub-block. The reference mean DTM shape is computed from 38 images with calibration conditions (i.e., using tight GPS and loose image constraints). The uncorrected sub-block is triangulated using 8 control points only (no GPS/IMU) and tight image constraints (Std Dev = (2[um]). The mean DTM shape deformation is computed by subtracting the DTM mean surface of the uncorrected test block from that of the reference block (see Figure 7). A similar procedure is repeated with the corrected sub-block: a test block of 38 images has been reprocessed in the DMC PPS with a correction grid applied and re-triangulated following the same procedure applied to the block of uncorrected photos. The attenuation of DTM bending in this case is 3.36 times (see Figure 8).

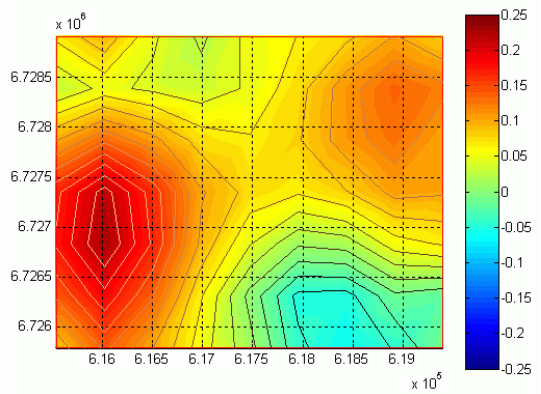

Figure 7. Block DTM bending in Z (uncorrected block – reference block) max=0.226[m]

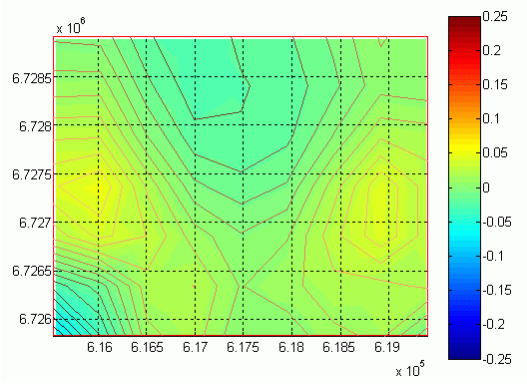

Figure 8. Block DTM bending in Z (reprocessed block – reference block) max=0.067[m]

5.1.3 Analysis of Collocation Grid versus Self-Calibration Grid

Self-calibration bundle adjustment using 44-parameter polynomials (Gruen, 1978) is also performed on the DMC 50 block. Significant APs are used to generate the correction grid. The

mean trend difference between DTMs computed with collocation and self-calibration is given in Figure 9.

Since the maximal mean difference is 4[cm], which is within the precision of the method, we can conclude that both adjustments enforce virtually the same block geometry. However, the same cannot be said about the image space where self-calibration estimates have a quite different distortion pattern due to inherent stiffness of the polynomial models (see Figure 10).

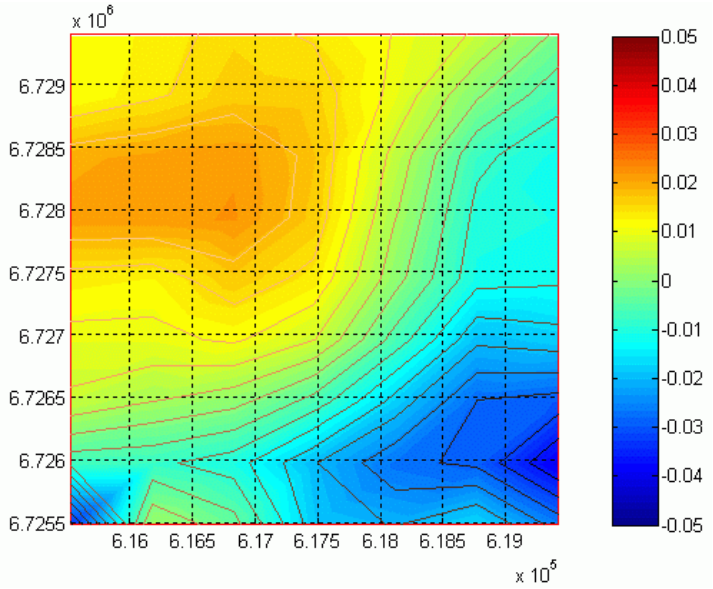

Figure 9. Mean DTM trend difference, max=0.04[m]

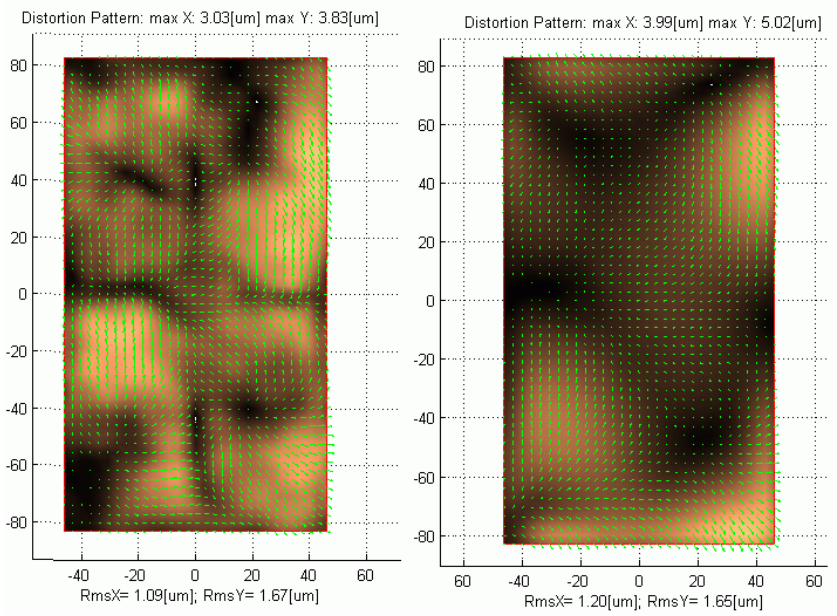

Figure 10. DMC 50 collocation grid versus self-calibration Grid

In total, the maximal difference between two grids is equal to 5[um], which means that self-calibration overcorrects (on the edges) almost a half pixel. So, the price to pay for correcting the block geometry in object space for self-calibration is to have significant systematic error in image

space, much larger than the initial systematic error. Such overcorrection at the edges may pose significant problems for assembly of ortho mosaics. However, both grids shown in Figure 10 produce virtually identical results on the test block used in Section 5.1.2., see table 4.

Table 4. Bundle adjustment statistics of DMC 50 sub-block with control points

Adjustment Type and Statistics	**No Grid** Sigma = 2.4[um] RMS x =1.7, RMS y =1.6			**Collocation Grid** Sigma = 2.3[um] RMS x = 1.7, RMS y = 1.5			**Self-Calibration Grid** Sigma = 2.3[um] RMS x = 1.7, RMS y = 1.5		
	X[m]	Y[m]	Z[m]	X[m]	Y[m]	Z[m]	X[m]	Y[m]	Z[m]
RMS of 8 Control Points	0.007	0.008	0.003	0.004	0.007	0.002	0.004	0.007	0.003
RMS of 6 Check Points	0.036	0.022	0.107	0.027	0.017	0.036	0.025	0.020	0.042
MAX of 8 Control points	0.012	0.016	0.005	0.008	0.012	0.004	0.007	0.015	0.006
MAX of 6 Check Points	0.074	0.044	0.160	0.053	0.023	0.063	0.050	0.033	0.065

5.2 DMC 48 Calibration and Testing

A procedure similar to that for the DMC 50 block has been conducted for the DMC 48 block. A few plots demonstrating calibration conditions and results are given in Figure 11.

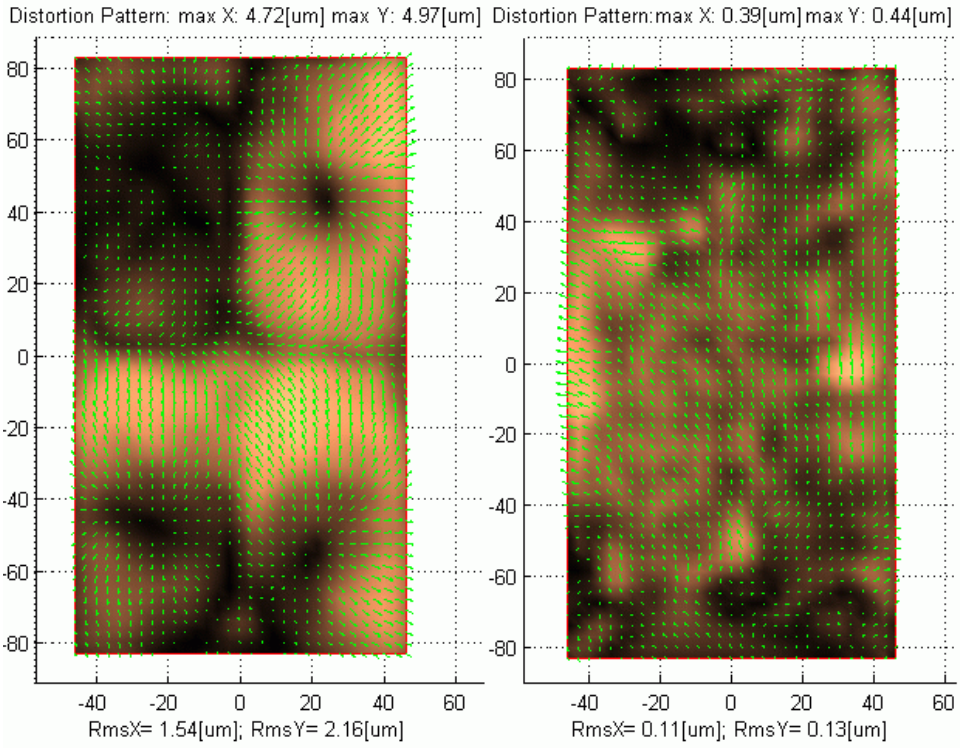

Figure 11. DMC 48 VIR correction grid and the remaining distortion trend

Again, in lieu of a separate test block, a reference sub-block is employed. This sub-block has 89 images with 60/60 % overlap configuration. The reference mean DTM shape is computed from

this sub-block using tight GPS and loose image constraints. The uncorrected sub-block is also triangulated with 21 control points only (no GPS/IMU) and tight image constraints (Std Dev = (2[um]). The mean DTM shape deformation is computed by subtracting the DTM mean surface of the uncorrected test block from that of the reference block. The same is done after the correction grid is applied to the test block. Results are shown in Figures 12 and 13. The attenuation of DTM bending is 5.5 times. The expected attenuation for any other test project is about 2 times due to large project-dependent part of the systematic error.

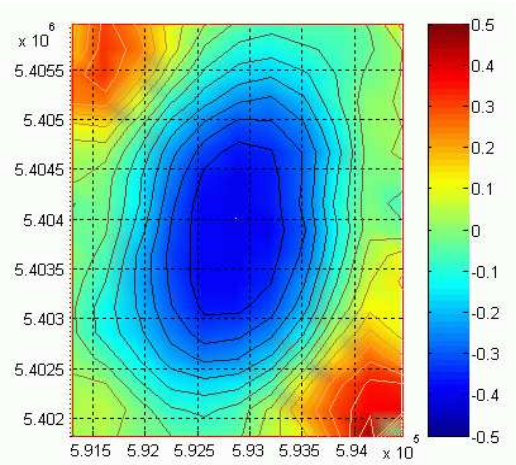

Figure 12. Block DTM Bending in Z (uncorrected block – reference block), (max=0.44[m])

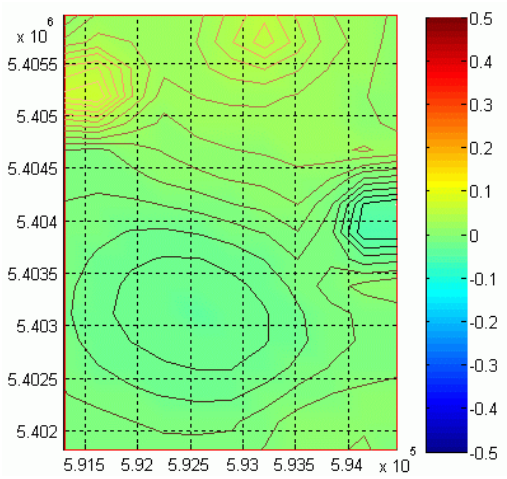

Figure 13. Block DTM Bending in Z (corrected block – reference block), (max=0.08[m])

5.3 DMC 27 Calibration and Testing

A procedure similar to that for the DMC 50 block has also been conducted for the DMC 27 block. A few plots demonstrating calibration conditions and results are given in Figure 14.

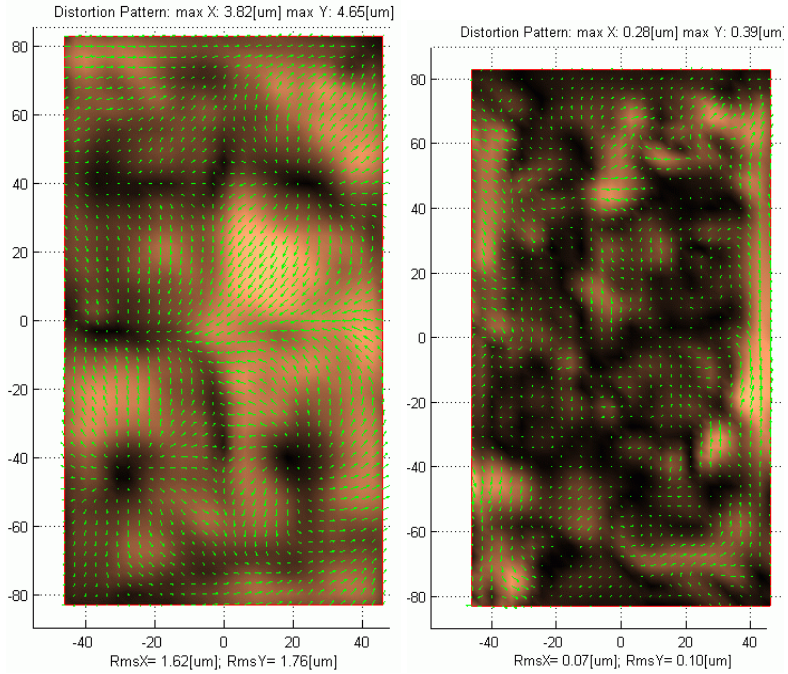

Figure 14. DMC 27 VIR correction grid and the remaining distortion trend

In lieu of a separate test block, the whole reference block (used in calibration) is employed. The reference mean DTM shape is computed from the calibration block (using tight GPS constraints and loose image constraints). The uncorrected test block is triangulated using 39 control points only and tight image constraints (Std Dev = (2[um]). The mean DTM shape is computed using the triangulated XYZ of the test block. The mean DTM shape deformation is computed by subtracting the DTM mean surface of the uncorrected test block from that of the reference block (Figures 15 and 16). The same is done after the correction grid is applied to the test block. The attenuation of DTM bending is 4 times.

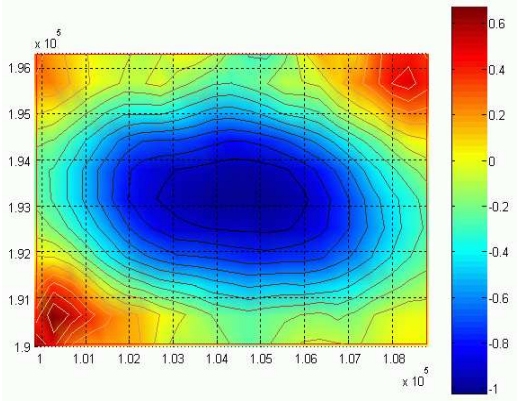

Figure 15. DTM Bending in Z
(uncorrected block – reference block)
max=1.02[m]

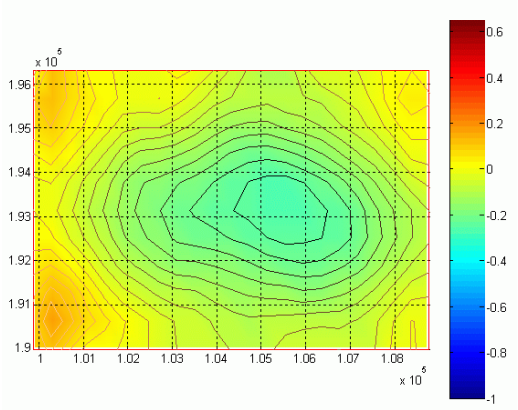

Figure 16. Block DTM Bending in Z
(corrected block – reference block)
max=0.26[m]

6. CONCLUSIONS AND FUTURE WORK

Three DMC cameras have been calibrated for VIR correction grid using collocation method. The DMC 50 block has also been used to compare the self-calibration grid to the collocation grid. Test sub-blocks of different configurations (regular 60/30 layout of 38 photos, 60/60 layout of 89 photos, and the whole calibration block of 1105 photos with 60/80 layout) have been used to measure the effect of DTM unbending by application of a VIR correction grid. The most reliable estimate of the unbending effect is the mean DTM trend difference between a GPS-constrained test block and unconstrained test block (sparse control at the edges of the block). This configuration produces the maximal block bending, and the mean DTM trend difference (and its maximum) serves as a robust estimate of the improvement in DTM shape. The robustly-computed mean trend is free from the effects of local deformation affecting sparsely distributed check points. The total attenuation of DTM bending on a sub-block selected from the calibration block ranges 3-5 times. The expected attenuation for any other block (flown at different GSD) is about 2 times due to the large project-dependent part of the systematic error. It is very important in the future to measure DTM bending on a block flown at different GSD than the one used to produce a single correction grid. In case such effect is significantly reduced, an array of correction grids needs to be computed to cover the span of all probable GSDs.

Another direction of future work is to capture the systematic distortion in the individual four PAN cameras by a collocation grid using a calibration flight with proper overlap of PAN camera footprints (i.e., all parallel strips flown in one direction). This work will take care of 35% of total DMC error. Another effort is to refine the geometric platform calibration procedure to significantly reduce the remaining 65% of DMC error by utilizing strong correlation of platform orientation parameters from exposure to exposure along a strip.

7. ACKNOWLEDEGEMENTS

This paper has been prepared with the use of several DMC blocks including “DMC 27” from Hansa Luftbild and “DMC 50” from LMV. We used these blocks for geometric correction analysis. The authors wish to thank the help of Hansa Luftbild, Flemish Geographical Information Agency (FGIA), and National Land Survey of Sweden (LMV) for supporting this research by providing their data.

8. REFERENCES

Alamús, R., Kornus W., Talaya, J. (2006): Studies on DMC Geometry. ISPRS Journal of Photogrammetry & Remote Sensing, Vol. 60, pp 375-386.

Dörstel C., 2007. DMC - (R)evolution on geometric accuracy, in: Fritsch D. (Ed.), Photogrammetric Week 2007, Wichmann, Heidelberg.

Dörstel C., 2003. DMC - Practical experiences and Photogrammetric System Performance, in: Fritsch D. (Ed.), Photogrammetric Week 2003, Wichmann, Heidelberg.

Grün, A. (1978): Progress in Photogrammetric Point Determination by Compensation of Systematic Errors and Detection of Gross Errors. International Society for Photogrammetry, Symposium of Commission III, Moscow, USSR.

Honkavaara, E., et. al. (2006): Complete Photogrammetric System calibration and Evaluation in the Sjökulla test field – Case Study with the DMC. In: EuroCow 2006 Proceedings Barcelona.

Jacobsen, K. (2007): Geometry and Information Contents of Large Size Digital Frame Cameras, ASPRS Annual Conference, Tampa, Florida, May 7-11, 2007.

Kruck, E. (2006): Simultaneous Calibration of Digital Aerial Survey Cameras. In: EuroCow 2006 Proceedings Barcelona.

Madani, M., Dörstel C., Heipke C., Jacobsen K. (2004): DMC practical experience and accuracy assessment. In: ISPRS Proceedings 2004 Istanbul.

Madani, M (2001). Z/I Imaging New Automatic Aerial Triangulation System, ASPRS Annual Conference, St. Louis, MO, April 23-27, 2001.

Madani M., (1985). Accuracy Potential of Non-Metric Cameras in Close-Range Photogrammetry Ph.D. Dissertation, Department of Geodetic Science and Surveying, The Ohio State University.

Riesinger, I (2006): Investigations on DMC (Digital Mapping Camera) Auto-Calibration, Diploma Thesis, Munich Technical University, Germany, 2006.

.